CHAPTER-2

Scope of Prussian blue analogue as a precatalyst for electrochemical water oxidation

2.1. Abstract

The electrochemical water oxidation demands the designing of active M(O)OH catalysts with tuned structural and electronic properties. Herein, we have adopted a unique method for the synthesis of a series of Fe-$Co(OH)_2$-Co(O)OH active catalysts by electrochemical reconstruction of CoFe-PBA. The chronoamperometric method with varying potential (1.45, 1.55, 1.65 V *vs* RHE) and time (12 and 24 h) has been applied for the anodic reconstruction of PBA and the effect of the applied anodic potential and time on the structure, morphology and catalytic performance of the active catalysts has been investigated. The electrochemically synthesized active catalyst AC-1 (prepared at 1.55 V *vs* RHE 12 h), having an atomic level thickness (~3 nm), high electrochemical surface area, exposed active sites, enhanced electronic conductivity, high mechanical stability, and strong catalyst-support interaction, produced the best water oxidation activity among the synthesized catalysts to deliver 10 mA cm^{-2} current density at 250 mV overpotential. Moreover, the stability of AC-1 was also recorded for 24 h under the CA conditions.

2.2. Introduction

Although tremendous progress has been achieved in the designing of transition metal-based electrocatalysts for electrochemical OER [221–223], the use of MOF as the precatalyst has been found to be beneficial to develop M(O)OH as active catalysts [64]. The MOF undergoes bulk anodic reconstruction to form ultrathin M(O)OH nanosheets. In contrast to the transition metal-derived other electrocatalysts, the bulk reconstruction of MOFs leads to the complete phase transformation, change of the morphology, composition tuning, and modulation of the electronic properties [46,61,181,224]. Previously, different research groups have demonstrated the bulk reconstruction of MOFs into active catalysts during the electrochemical OER [46,61,181,224].

For example, Duan et al. investigated the bulk reconstruction of NiFe-MOF under the anodic OER conditions to avail Ni(O)OH nanosheets [225]. The complete electrochemical reconstruction of various MOFs like NiCo-MOF and NiCoFe-MOF was also established during alkaline OER [226,227]. Further, bulk chronoamperometric reconstruction of CoFe-PBA to Co(O)OH nanosheets has been demonstrated by Zhou et al [179]. In another report, complete electrochemical reconstruction of NiFe-PBA into $Ni(OH)_2$ active catalyst has been established [180]. These studies have shown the excellent catalytic activities of M(O)OH active catalysts over the pristine MOFs.

Inspired by these reports, we have demonstrated a template-directed growth of self-supported CoFe-PBA precatalyst (PC-1) on carbon cloth. The self-supported CoFe-PBA has been prepared using the CoHC@CC template (Figure 2.1). The PBA provides a large surface area, high porosity, exposed facets, and tuned structural and electronic properties while the self-supported strategy offers high electronic conductivity, facile charge transport, and strong interaction between catalyst and support. Further, the complete and bulk reconstruction of PC-1 was performed under CA conditions forming a series of

active Fe-$Co(OH)_2$-Co(O)OH catalysts (denoted as AC-x, x = 1, 2, 3, 4 see table 2.1). The precatalyst and corresponding active catalysts have been characterized by spectroscopic and microscopic techniques.

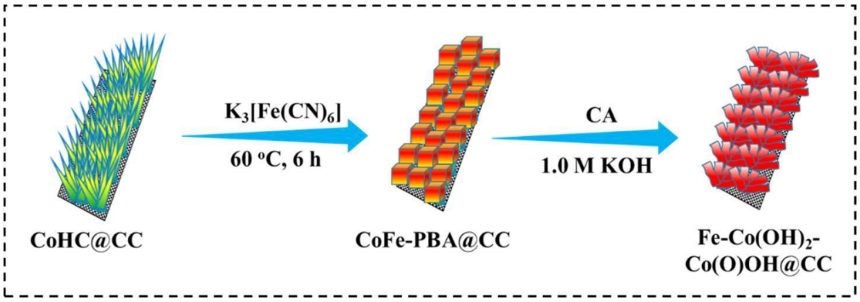

Figure 2.1. Schematic depiction for the synthesis of CoHC@CC templated CoFe-PBA@CC and its chronoamperometric reconstruction into ultrathin Fe-$Co(OH)_2$-Co(O)OH@CC.

The specific objectives of this work can be explained by:

(i) The effect of the varying anodic potentials (1.45 V, 1.55 V, and 1.65 V *vs* RHE) and time (12 h and 24 h) during the electrochemical transformation of CoFe-PBA into active catalysts has been investigated. The spectroscopic, microscopic, and analytical techniques have been utilized to understand the differences in active catalysts.

(ii) Further, the effect of the structural variation of the active catalysts (due to variation in the time and potential during the synthesis) on the water oxidation activity has been studied.

(iii) The best reaction condition for the synthesis of active catalysts has been investigated to get outstanding water oxidation activity.

(iv) The superiority of PBA-derived active Fe-$Co(OH)_2$-Co(O)OH catalysts has been established over the cobalt-based hydroxide (CoHC) and layered double hydroxide (CoFe-LDH) prepared by the hydrothermal method. The advantages of bulk

electrochemical reconstruction of PBA were established by comparing the catalytic activity of pristine PBA and corresponding active Fe-$Co(OH)_2$-Co(O)OH catalysts.

Interestingly, our study has shown that the change of the potential and time during the electrochemical reconstruction has resulted in the formation of active catalysts with the same phase [Fe-$Co(OH)_2$-Co(O)OH] and morphology (ultrathin nanosheets). The electrochemical reconstruction at 1.55 V *vs* RHE for 12 has been found to be optimum as AC-1 has demonstrated excellent water oxidation activity among the reconstructed catalysts. However, variation in the water oxidation activity of the active catalysts could be attributed to the different Fe content, Co^{4+}/Co^{3+} ratio as well as mechanical stability of the catalyst on the electrode surface. Moreover, our investigations have established that the PBA-derived Fe-$Co(OH)_2$-Co(O)OH has outpaced the hydrothermally prepared hydroxide and LDH in water oxidation activity.

2.3. Chemicals

Cobalt chloride hexahydrate ($CoCl_2.6H_2O$) and urea (NH_2CONH_2) were acquired from MERCK Life Sciences Ltd. (India). Ammonium fluoride (NH_4F) and potassium hexacyanoferrate(III) ($K_3[Fe(CN)_6]$) were procured from SRL Pvt. Ltd. India. The carbon cloth (CC) was purchased from Nara Cell Tech South Korea. Double distilled water was utilized for all the experiments.

2.4. Instruments

The crystal structure of the prepared catalysts was recorded using Rigaku Smart Lab 9 kW powder X-Ray diffractometer with Cu K_α radiation (λ=1.5418 Å). Further, the Fourier transform infrared (FTIR) spectroscopy was executed in attenuated total reflectance (ATR) mode using a Thermo Scientific Nicolet iS5 spectrometer. The electronic valence states of the elements were examined using an X-ray photoelectron spectrometer from VG/VG ESCA LAB 220i while the XPS 4.1 software was used for the

deconvolution of XPS. The morphological properties of the catalysts were analyzed using field emission scanning electron microscope EVO-Scanning Electron Microscope MA15/18 and Tecnai G2 20 TWIN transmission electron microscope. The autolab potentiostat/galvanostat (Model PGSTAT-72637) was utilized for the electrochemical characterization. Energy dispersive X-ray (EDX) was analyzed with Team Pegasus Integrated EDS-EBSD.

2.5. Experimental

2.5.1. Synthesis of cobalt hydroxide carbonate on carbon cloth [81]

First, the pieces of CC (1 cm × 2 cm) were thoroughly washed with acetone and water. Further, the CC was activated by treating with conc. HNO_3 at 100 ^oC for 4 h. After cooling down, the activated CC was washed with H_2O three times and subsequently dried at 50 ^oC in an air oven for 12 h. In the next step, $CoCl_2.6H_2O$ (2 mmol) was added to 12 mL water and stirred for 10 minutes to get a clear solution. Next, NH_4F (4 mmol), and NH_2CONH_2 (10 mmol) were added to the $CoCl_2$ solution and stirred for 20 minutes. The mixture was placed in a Teflon-lined autoclave and the pieces of CC were vertically placed in such a way that 1 cm^2 area was dipped inside the mixture. The autoclave was sealed and placed into an air oven preheated at 120 ^oC. The reaction was continued for 5 h followed by natural cooling. The CoHC deposited CC films were taken out from the autoclave and washed with distilled H_2O and ethanol and dried for 12 h at 50 ^oC.

2.5.2. Preparation of CoFe-PBA on carbon cloth (PC-1)

The PBA precatalyst was prepared by treating CoHC@CC with $K_3[Fe(CN)_6]$. In particular, a single CoHC@CC film was placed inside a glass vial containing a solution of 0.2 mmol $K_3[Fe(CN)_6]$ in H_2O (5 mL). The film in the solution was aged for one hour at room temperature, followed by a heat treatment in an oven at 60 ^oC for 6 h. After natural

cooling, the CoFe-PBA deposited CC film was taken out from the vial and washed with H_2O for three times, and dried at 50 ^oC for 12 h.

2.5.3. Synthesis of CoFe-LDH@CC

The CoFe-LDH@CC was developed using a hydrothermal approach. In the first step, 1 mmol $CoCl_2.6H_2O$ and 1 mmol $FeCl_2.4H_2O$ were mixed into 12 mL H_2O followed by the addition of 4 mmol of NH_4F and 10 mmol of NH_2CONH_2. The mixture was stirred for 20 minutes to form a homogeneous solution and then transferred in a Teflon-lined autoclave. The pieces of CC were kept inside the solution in a vertical condition so that 1 cm^2 area of CC was immersed inside the solution. The autoclave was sealed and put inside the oven at 120 ^oC. The reaction was carried out for 5 h. After natural cool down, CoFe-LDH@CC films were removed from the autoclave and washed with distilled H_2O and ethanol three times and subsequently dried for 12 h at 50 ^oC.

2.5.4. Fabrication of RuO_2 on CC

The RuO_2 was purchased from Sigma Aldrich. 2 mg RuO_2 was dispersed in a 200 µL solution containing 100 µL water, 50 µL ethanol, and 50 µL of 0.5 wt.% Nafion solution. The solution was sonicated for 10 min to form a homogeneous mixture. The mixture was drop cast on carbon cloth by taking 25 µL solution every time and drying at 50 °C for 10 min. After the complete deposition, the catalyst film was dried at 50 °C in an air oven for 6 h.

2.6. Electrochemical measurements

All the electrochemical experiments were performed in a single electrochemical cell with three electrodes in a 1.0 M aqueous KOH solution (pH 13.9). The reconstructed catalyst on CC was employed as a working electrode while Pt wire was implemented in form of a counter electrode. Further, Ag/AgCl was utilized in form of a reference electrode. The CV and LSV profiles were recorded at the scan rate of 2 mV s^{-1} and presented in the

thesis with 80% iR correction. The potential was presented against the reversible hydrogen electrode (RHE) by the following equation:

$$E(RHE) = E(Ag/AgCl) + 0.197 + 0.059pH$$

The EIS studies were performed in the range of 0.001 to 100,000 Hz frequency with the 10 mV amplitude. The diameter of the semicircle in the EIS plot was utilized for the R_{ct} determination. The CA was measured at a constant potential for a fixed time. The overall water splitting activity was measured in a two-electrode electrolyzer single-compartment cell.

2.7. Results and discussion

2.7.1. Characterization of precatalyst PC-1

The precatalyst PC-1 was first characterized by PXRD to investigate the crystal structure. The PXRD pattern of PC-1 revealed that the PC-1 had a cubic crystal structure with an *Fm3m* space group (Figure 2.2a). In PC-1, the Co centers are connected to the N atom while Fe centers are bonded with the C atom of –CN bridges forming a cubic framework. The PXRD pattern was matched with the standard reference data of JCPDF No-01-077-1116. The IR spectroscopy provided the first indication for the formation of PC-1. The two intense peaks at 2170 cm^{-1} and 2130 cm^{-1} were originated from the asymmetric stretching vibrations of –CN groups in PC-1 (Figure 2.2b) [228].

The electronic valence state of the elements in PC-1 was studied by the XPS technique. The peaks at the 781.5 eV and 797.3 eV in Co 2p spectrum of PC-1 were identified for Co $2p_{3/2}$ and Co $2p_{1/2}$, respectively (Figure 2.2c) [65,81,103,151,229]. The peak at 781.5 eV indicated the presence of Co^{2+} species in PC-1. The spin-orbit coupling spacing of 15.8 eV further supported that the Co^{2+} was the dominant species in PC-1 [103,148,151]. Further, the peaks for Fe $2p_{3/2}$ and Fe $2p_{1/2}$ were originated at 708.3 eV and 721.1 eV, respectively in PC-1 (Figure 2.2d). The Fe 2p XPS confirmed the presence

of Fe^{3+} in PC-1 [230]. The C 1s XPS reflected the different peaks at 288.1 eV, 286.1 eV, and 284.3, which were assigned to the C=N, C-N, and C=C bonding in PC-1, respectively (Figure 2.2e) [231]. Further, the fitting of N 1s XPS of PC-1 resulted in the three peaks at 400.1 eV, 398.4 eV, and 397.4 eV, attributed to the C-N, C=N, and C≡N, respectively (Figure 2.2f) [231]. Furthermore, the O 1s XPS of PC-1 showed two prominent peaks at 531.7 eV for adsorbed H_2O and 530.9 eV for surface –OH groups (Figure 2.2g) [64,65,81,152].

Further, SEM was employed to analyze the morphological features of PC-1. The cubic particles with varying sizes were detected in SEM images of PC-1 (Figure 2.2h). The morphology of PC-1 was further demonstrated using TEM studies. TEM image further established the cubic morphology of the PC-1 (Figure 2.2i). A characteristic d-spacing of 0.51 nm was identified in the HRTEM image, which was correlated to the (200) plane of PBA (JCPDF No-01-077-1116) in PC-1 (Figure 2.2j). The crystalline nature of PC-1 was observed in the SAED pattern (Figure 2.2j inset). The EDX spectroscopy revealed the presence of Co, Fe, C, and N in PC-1 (Figure 2.2k).

2.7.2. Electrochemical reconstruction of PC-1 into active catalysts

The electrochemical bulk reconstruction of precatalyst PC-1 was carried out in a single cell with three electrodes set up in 1.0 M KOH solution. The PC-1 was employed as the working electrode while Pt wire was the counter electrode and Ag/AgCl was the reference electrode. The CA was performed at three different potentials 1.55 V, 1.45 V, and 1.65 V *vs* RHE for a fixed time of 12 h to synthesize active catalysts AC-1, AC-2, and AC-3, respectively (Table 2.1). Further, the time was also changed to 24 h at a constant potential of 1.55 V *vs* RHE to form AC-4 (Table 2.1).

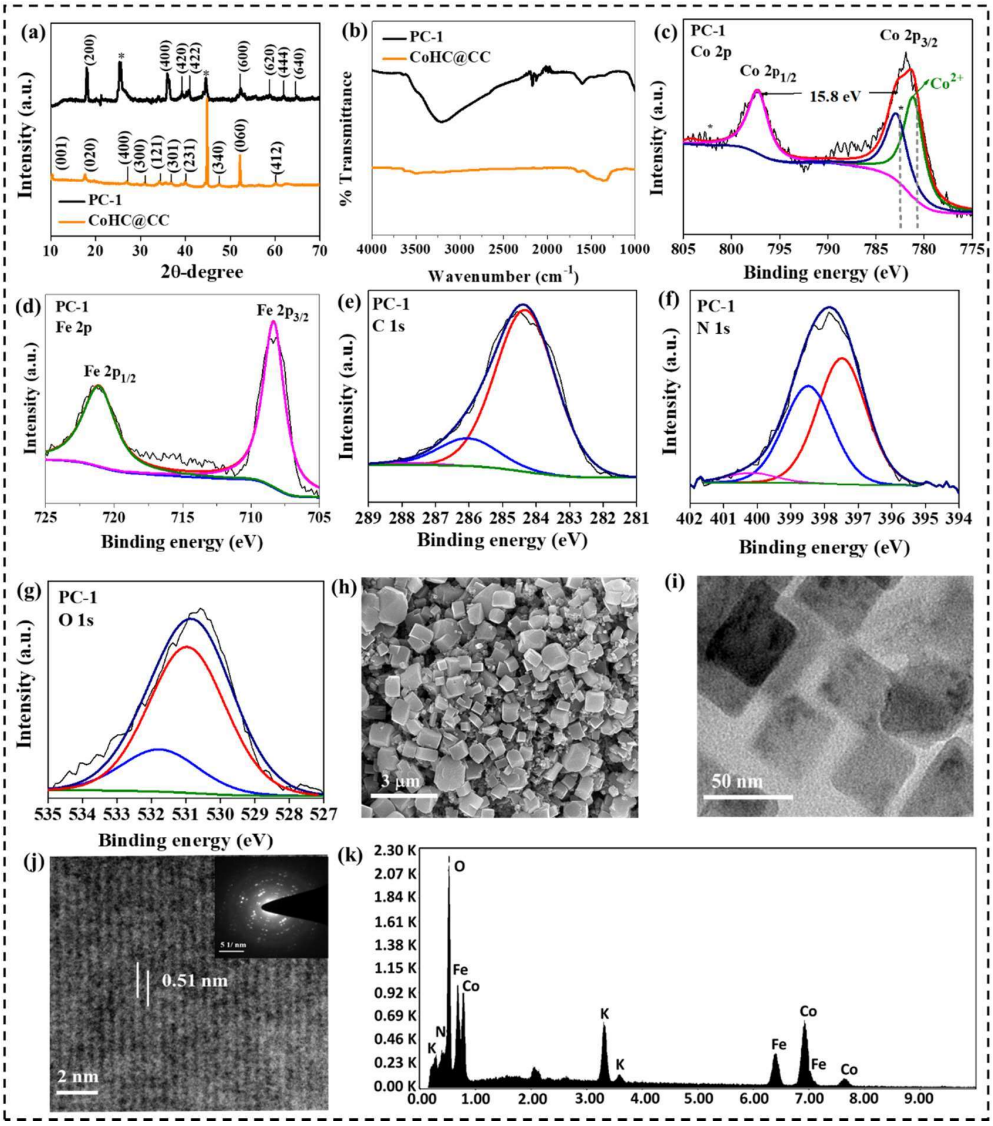

Figure 2.2. (a) PXRD pattern of CoHC@CC and PC-1; (b) IR spectra of CoHC@CC and PC-1; (c) Co 2p XPS of PC-1; (d) Fe 2p XPS of PC-1; (e) C 1s XPS of PC-1; (f) N 1s XPS of PC-1; (g) O 1s XPS of PC-1; (h) SEM image of PC-1; (i) TEM image of PC-1; (j) HRTEM image of PC-1 (SAED inset) and (k) EDX spectra of PC-1.

Table 2.1. Details of various active catalysts synthesized by CA treatment of PC-1.

Precatalyst	Active catalyst	Denoted name	Reaction conditions
PC-1	Fe-Co$(OH)_2$-Co(O)OH	AC-1	1.55 V *vs* RHE, 12 h
PC-1	Fe-Co$(OH)_2$-Co(O)OH	AC-2	1.45 V *vs* RHE, 12 h
PC-1	Fe-Co$(OH)_2$-Co(O)OH	AC-3	1.65 V *vs* RHE, 12 h
PC-1	Fe-Co$(OH)_2$-Co(O)OH	AC-4	1.55 V *vs* RHE, 24 h

2.7.3. Characterization of the active catalysts

The precatalyst PC-1 was reconstructed electrochemically under the CA by varying the potential and time. The bulk reconstruction of PC-1 rendered a series of Fe-$Co(OH)_2$-Co(O)OH active catalysts (Figure 2.3a). The formation of the active catalysts was established by spectroscopic and microscopic studies (see further). Firstly, IR spectra of reconstructed catalysts suggested that the bulk reconstruction of PC-1 led to the complete loss of the peaks for bridging –CN groups to form a new structure (Figure 2.3b) [81]. Further, the PXRD pattern of all the active catalysts demonstrated the peaks for the α-$Co(OH)_2$ (JCPDF No-48-0083) and β-Co(O)OH (JCPDF No-26-0480) indicating the mixed phase structure (Figure 2.3c).

The PXRD studies revealed a similar structure of all the reconstructed active catalysts. The variation in the potential and time did not affect the structure of the reconstructed active catalysts. As the excellent OER activity was furnished by AC-1, further characterization was performed with AC-1. The electronic states of various elements in AC-1 were detected by XPS. The Co 2p XPS identified the peaks for Co $2p_{3/2}$ and Co $2p_{1/2}$ at 780.2 eV and 795.3 eV, respectively (Figure 2.3d) [81,103,148,151,161,229]. The two peaks for Co^{3+} and Co^{2+} in AC-1 were appeared at 780.3 eV and 781.3 eV, respectively. A significant reduction in the spin-orbit coupling spacing was identified in AC-1 (15.2 eV) in contrast to PC-1 (15.8 eV). The decrease in spin-orbit coupling spacing and origination of the peak of Co^{3+} established that the bulk reconstruction led to the oxidation of metal ions [81,103,148,151,161,229]. Further, Fe 2p XPS displayed two intense peaks at 708.7 eV and 721.6 eV assigned to the Fe $2p_{3/2}$ and Fe $2p_{1/2}$, respectively (Figure 2.3e). The presence of the peaks at 708.8 eV and 710.8 eV confirmed the Fe^{2+} and Fe^{3+} in AC-1, respectively [230]. The two peaks were emerged at 532.5 eV for adsorbed H_2O and 531.4 eV for surface –OH whereas a third peak was

identified at 530.4 eV for the metal-oxygen bond in AC-1 (Figure 2.3f) [40,81,148]. The presence of a peak for the metal-oxygen bond confirmed the formation of the $Co(OH)_2$-Co(O)OH structure.

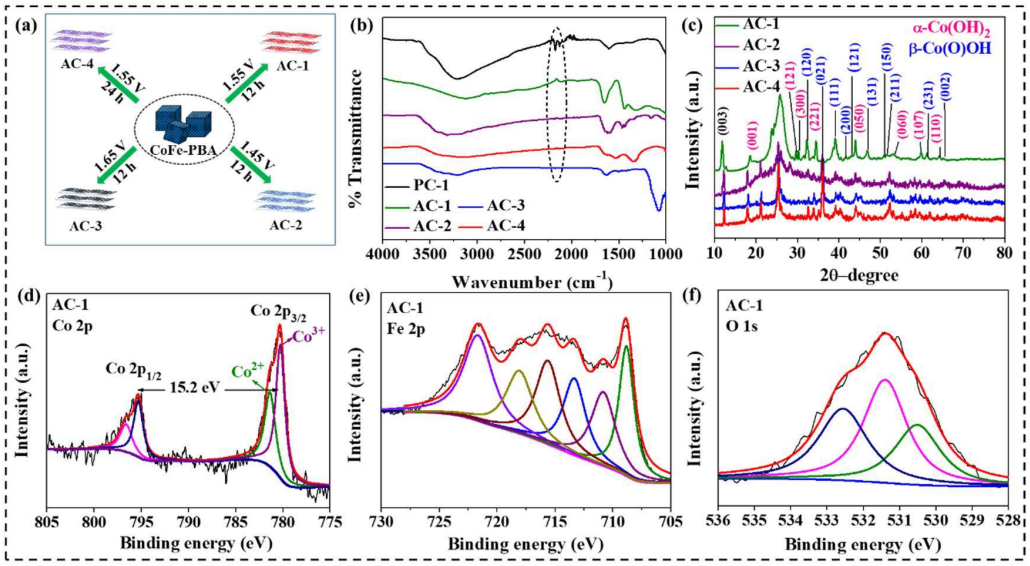

Figure 2.3. (a) Schematic illustration for the chronoamperometric synthesis of AC-1, AC-2, AC-3, AC-4 from CoFe-PBA@CC; (b) IR spectra of AC-1, AC-2, AC-3, AC-4 compared with PC-1; (c) PXRD pattern of AC-1, AC-2, AC-3, AC-4; (d) Co 2p XPS of AC-1; (e) Fe 2p XPS of AC-1 and (f) O 1s XPS of AC-1.

SEM image indicated the ultrathin nanosheets of AC-1 (Figure 2.4a-b). However, the determination of the actual thickness of the nanosheets by SEM could be erroneous. Therefore, AFM studies were performed, which showed that the ultrathin nanosheets of AC-1 had a thickness of ~3 nm (Figure 2.4c). The Tyndall effect experiment also evidenced the existence of ultrathin nanosheets (Figure 2.4d). TEM images established that all the active catalysts possessed ultrathin nanosheet morphology having an atomic level thickness (Figure 2.4e-h). The d-spacing of 0.44 nm was identified for the (002) plane of β-Co(O)OH (JCPDF No-26-0480) in AC-1 (Figure 2.4i). SAED pattern of AC-1

confirmed the crystalline nature of the active catalyst (Figure 2.4i inset). Similarly, HRTEM image of AC-2 showed 0.40 nm d-spacing for (110) plane of α-$Co(OH)_2$ (Figure 2.4j) while AC-3 and AC-4 identified the 0.46 nm lattice spacing related to the (100) plane in α-$Co(OH)_2$ (JCPDF No-02-0925) (Figure 2.4k-l). It can be concluded that all the reconstructed active catalysts have similar structures and morphology.

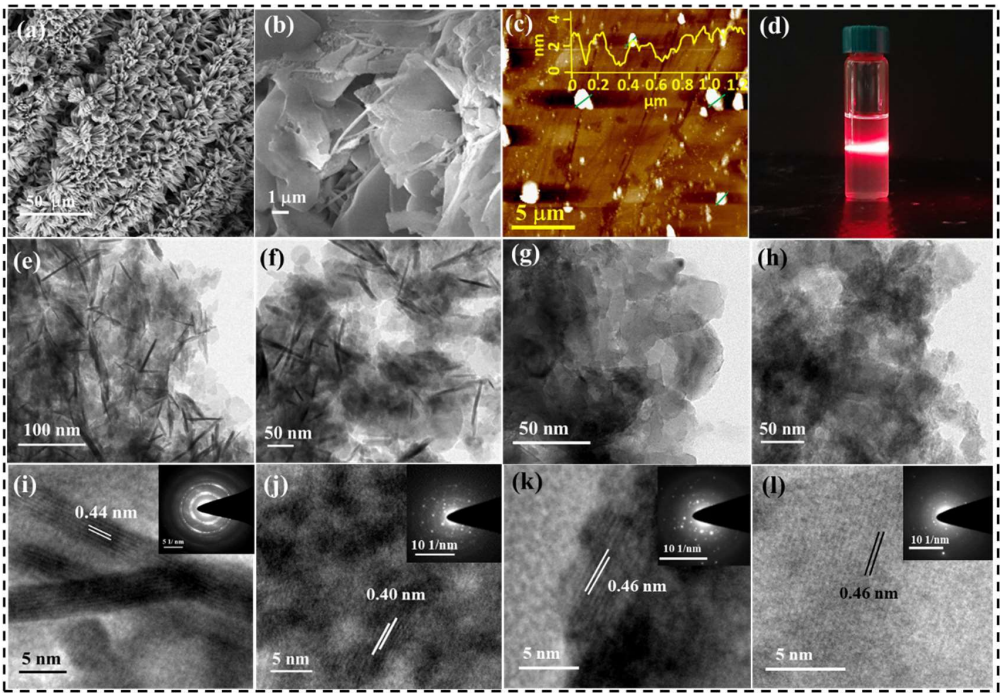

Figure 2.4. (a-b) SEM images of AC-1 at different resolutions; (c) AFM topography image of AC-1 (inset height ptofile); (d) image of Tyndall effect experiment with AC-1; (e) TEM image of AC-1; (f) TEM image of AC-2; (g) TEM image of AC-3; (h) TEM image of AC-4; (i) HRTEM image of AC-1 (SAED inset); (j) HRTEM image of AC-2 (SAED inset); (k) HRTEM image of AC-3 (SAED inset) and (l) HRTEM image of AC-4 (SAED inset).

Further, the dissolution of Fe from the PC-1 precatalyst was observed during the CA reconstruction. ICP-AES studies revealed that the AC-1 possessed 5-8% Fe content in the

structure. XPS analysis also confirmed that Fe was leached out in the electrolyte from PC-1 during the reconstruction process. The Fe leaching was also reported during the electrochemical reconstruction in previous studies [179,180,225,232].

2.7.4. Electrochemical performance of the active catalysts

The electrochemical OER performance of the reconstructed catalysts was studied in an alkaline medium (pH 13.8). Firstly, a short CV profile found the redox peak for the oxidation of Co^{2+} to Co^{3+} in AC-1 during OER (Figure 2.5a) [84]. Among the studied catalysts, AC-1 demonstrated outstanding OER performance at the input of 250 mV overpotential to reach an anodic current density of 10 mA cm^{-2} (Figure 2.5b). In contrast, the AC-2 and AC-3 required overpotentials of 270 mV and 300 mV to deliver the same current density, respectively. Moreover, AC-4 realized 300 mV overpotential to afford an anodic current density of 10 mA cm^{-2}. The comparison of the CV profile established that the AC-1 showed remarkable improvement in the water oxidation activity in contrast to the PC-1 ascribed to the bulk electrochemical reconstruction (Figure 2.5b).

The catalyst AC-1 performed better OER activity in comparison to CoHC@CC (370 mV) and CoFe-LDH@CC (330 mV) bulk material (Figure 2.5b). Moreover, AC-1 outperformed the noble metal-based RuO_2 catalyst signifying the excellent water oxidation activity (Figure 2.5b). These results clearly demonstrated the superiority of the electrochemically reconstructed Fe-doped $Co(OH)_2$-Co(O)OH over the LDHs prepared by the hydrothermal method. The reconstructed AC-1 established better or comparable OER performance with PBA-derived electrocatalysts and the self-supported electrocatalysts investigated in the literature.

The reaction kinetics of the reconstructed catalysts for OER was assessed from the Tafel plots. The active catalyst AC-1 reflected the smallest value of Tafel slope (57 mV dec^{-1}) among the synthesized catalysts suggesting the improved water oxidation kinetics

(Figure 2.5c). The long-term stability of AC-1 was evaluated under CA conditions. The AC-1 revealed excellent stability for 24 h at a fixed potential of 1.49 V *vs* RHE without a significant drop in OER current density (Figure 2.5d).

The outstanding OER activity of AC-1 was explained on the basis of improved charge transport kinetics and the ECSA. The smaller value of charge transfer resistance (R_{ct}) was determined in the EIS plot for AC-1 compared to hydrothermally prepared CoHC@CC (Figure 2.5e). The lower R_{ct} suggested the improved charge transfer kinetics of electrochemically reconstructed AC-1 than the CoHC@CC. Furthermore, the ECSA of AC-1 was measured to be 20.25 cm^2, which was three times greater than the CoHC@CC (6.5 cm^2) (Figure 2.5f). The larger ECSA of AC-1 suggested the larger number of exposed active sites, which promoted the binding of water on the surface to enhance the OER performance.

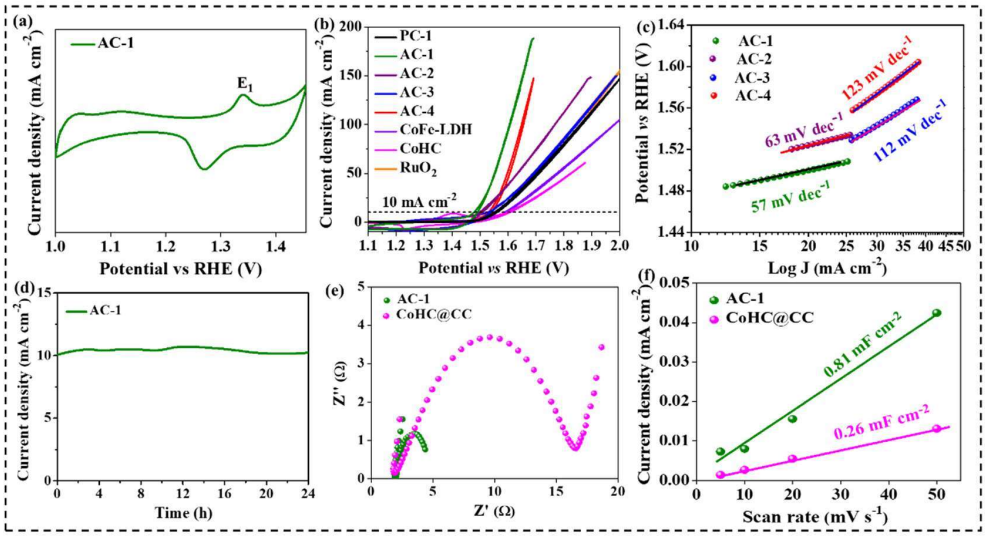

Figure 2.5. (a) CV profile of AC-1 during OER; (b) CV profiles for the OER activity of AC-1, AC-2, AC-3, AC-4 compared with PC-1, CoHC@CC, CoFe-LDH@CC, RuO_2@CC; (c) Tafel plots of AC-1, AC-2, AC-3, AC-4; (d) CA stability test of AC-1 for 24 h; (e) EIS plots of AC-1 compared with CoHC@CC and (f) C_{dl} measurements of AC-1 compared with CoHC@CC.

The variation in the OER activity of the reconstructed active catalysts can be explained on the basis of variation in the Co^{4+}/Co^{3+} ratio, different amounts of Fe, and peeling of the precatalyst during reconstruction. As the AC-1 was synthesized at 1.55 V *vs* RHE, it possessed a high ratio of Co^{4+}/Co^{3+} compared to the AC-2 synthesized at 1.45 V *vs* RHE. As a result, AC-1 showed better catalytic activity for water oxidation compared to AC-2. Although AC-3 and AC-4 exhibited a high ratio of Co^{4+}/Co^{3+}, the peeling of the catalyst occurred during the reconstruction at a high potential (1.65 V *vs* RHE) and long time (24 h). This ultimately led to poor catalytic performance for AC-3 and AC-4.

2.8. Conclusions

In summary, we have established a unique chronoamperometric strategy for the bulk reconstruction of PBA to form a series of active Fe-$Co(OH)_2$-Co(O)OH catalysts. The potentials and time during the chronoamperometric transformation were varied to find out the best reaction condition to attain excellent OER activity. Interestingly, the electrochemically synthesized AC-1 catalyst (CA for 12 h at 1.55 V *vs* RHE) demonstrated the best water oxidation activity among the studied catalysts. The spectroscopic and microscopic investigations established that the variation in anodic potential and time during the transformation rendered Fe-α-$Co(OH)_2$-β-Co(O)OH structure with the morphology of ultrathin nanosheet for all the reconstructed catalysts. The OER activity of the reconstructed catalysts was varied among the catalysts due to the different Co^{4+}/Co^{3+} ratios, presence of the different amounts of Fe as well as peeling of the precatalyst during bulk reconstruction.